ARTICLE

Induced pluripotent stem cell-derived vascular networks to screen nano-bio interactions

Luís Estronca[a], Vitor Francisco[b], Patrícia Pitrez[b], Inês Honório[b], Lara Carvalho[c], Helena Vazão[b], Josephine Blersh[b], Akhilesh Rai[a], Xavier Nissan[d], Ulrich Simon[e], Mário Grãos[b], Leonor Saúde[c] and Lino Ferreira[a]*

The vascular bioactivity/safety of nanomaterials is typically evaluated by animal testing that is low throughput and does not account for biological differences between animals and humans such as ageing, metabolism and disease profile. The development of personalized human *in vitro* platforms to evaluate the interaction of nanomaterials with the vascular system would be important for both therapeutic and regenerative medicine. A library of 30 nanoparticle (NP) formulations, in use in imaging, antimicrobial and pharmaceutical applications, was evaluated in a reporter zebrafish model of vasculogenesis and then tested in personalized humanized models composed by human induced pluripotent stem cells (hiPSCs)-derived endothelial cells (ECs) with a "young" and "aged" phenotypes in 3 vascular network formats: 2D (in polystyrene dish), 3D (in Matrigel) and in a blood vessel on a chip. As a proof of concept, vascular toxicity was used as the main readout. The results show that the toxicity profile of NPs to hiPSC-ECs was dependent on the "age" of the endothelial cells and vascular network format. hiPSC-ECs were less susceptible to the cytotoxicity effect of NPs when cultured in flow than in static conditions, being the protective effect mediated, at least in part, by the glycocalyx. Overall, the results presented here highlight the relevance of in vitro hiPSC-derived vascular systems to screen vascular nanomaterial interactions.

1. Introduction

Nanomaterials and nanomaterials-based technologies enable the development of new materials and applications across disciplines, including mechanical and electrical engineering, agriculture, energy generation and medicine.[1-3] The interaction of these nanomaterials with the human body are only partially known.[4-6] The development of new cell-based platforms for the rapid profiling of nanomaterials in terms of bioactivity, toxicity, biodegradation, among other aspects, is of great need.[7, 8] The majority of the nanomaterials that enter the human body, independently on the route of entry, will certainly circulate and be transported in the vascular system through the blood vessels and therefore it is critical to study their impact in individuals with differences in their vascular biology because of their genetic background or pathologies. The effects of nanomaterials in the disruption of the integrity of endothelial cell-cell communication[9] and in the induction of endothelial[10] and smooth muscle[11] cell toxicity have been identified.

Standard protocols for assessing the effect of nanomaterials on the vascular system involve testing in animals.[5, 10] Unfortunately, these tests are low-throughput, expensive, yield limited mechanistic information, do not address the current policies of regulatory agencies to alternate animal testing, and do not account for differences between species. Moreover, with the advent of personalized medicine, new cell technologies are required to provide patient-specific information about nanomaterial bioactivity/safety. In this respect, human induced pluripotent stem cells (hiPSCs) represent a potential source of endothelial (ECs) and smooth muscle cells (SMCs).[12-14] These humanized systems are, in some aspects, superior to animal models because they recapitulate human ageing, metabolism as well as disease profile. Unfortunately, hiPSC-derived ECs and SMCs have not been used to study the bioactivity/safety of nanomaterials along different individuals. These cells may be cultured under flow shear conditions in microfluidic systems to better mimic the *in vivo* conditions.

In this work, the impact of nanomaterials in iPSC-derived vascular networks was evaluated in 2D, 3D and blood vessel on a chip *in vitro* models. While the first two models run in static conditions, the blood vessel on a chip model runs in flow conditions, similar to *in vivo* conditions, which allows the formation of a functional glycocalyx layer on top of endothelial cells. Thirty nanomaterials that are normally used for different applications such as clinical molecular imaging, protective formulations, antimicrobial coatings, pharmaceutical

a. *Faculty of Medicine, University of Coimbra, 3000-548, Coimbra, Portugal.*
b. *Center for Neuroscience and Cell Biology, University of Coimbra, Coimbra, Portugal.*
c. *Instituto de Medicina Molecular e Instituto de Histologia e Biologia do Desenvolvimento, Faculdade de Medicina da Universidade de Lisboa, 1649-028, Lisboa, Portugal.*
d. *CECS, I-STEM, AFM, Institute for Stem Cell Therapy and Exploration of Monogenic diseases, Evry cedex, France.*
e. *Institute of Inorganic Chemistry, RWTH Aachen University, Germany.*
* *Email: lino@uc-biotech.pt*

formulations and catalysts have been selected (Figure 1). The nanomaterials with a metallic or polymeric composition and sizes ranging between 1.4 and 400 nm were initially tested in the zebrafish embryo vasculogenesis/angiogenesis to investigate their *in vivo* effect. Subsequently, the nanomaterials were tested in the *in vitro* human iPSC-derived vascular networks from two individuals in the same timeframe as the zebrafish tests (i.e. 24 h) to evaluate their acute toxicity. One of the iPSC line was derived from fetal cells (cord blood of an healthy newborn) while the other was generated from fibroblasts of a 14 years old female patient with Hutchinson-Gilford Progeria Syndrome (HGPS).[15] HGPS is a rare and fatal disease caused by a single point mutation of the LMNA gene leading to the accumulation of an abnormally truncated Lamin A protein called Progerin, which in turn leads to accelerated ageing.[16] The accumulation of Progerin is also observed during

Figure 1 - **NP library and *in vivo/in vitro* models to screen their toxicity. (A)** Properties of the NPs. The NPs can be categorized based on their size as: ultrasmall (3 NPs) or small (27 NPs); based on their composition as: inorganic (15 NPs) or organic (15 NPs); and by the type of the coating: peptides (3), polymers (2), functional groups (4) or anti-oxidants (2). **(B)** *In vivo* and *in vitro* models to screen NP toxicity. *In vivo model*: 30 NPs were tested at 1 μg/mL in 4hpf zebrafish embryos (manual dechorionated) for 24 h. The readout was vasculogenesis. *2D model* (in culture plates, static conditions): 30 NPs were incubated at 4 different concentrations (6, 12.5, 25 and 50 μg/mL) for 24 h with N-iPSC ECs or HGPS-iPSC ECs. The readouts were: (i) cell survival and (ii) nanomaterial internalization. *3D model* (in Matrigel, static conditions): 30 NPs were incubated at 2 concentrations (12.5 and 25 μg/mL) together with iPSC ECs in culture plates with Matrigel for 24 h. The readouts were: (i) length of microvessels formed, (ii) cell survival and (iii) gene expression. *Blood vessel on a chip* (microfluidic system; flow conditions): 10 NPs were tested at 50 μg/mL in arterial flow conditions in a co-culture of N-iPSC SMCs and N-iPSC ECs for 24 h. The readout was: (i) cell survival.

physiological ageing, although at much low levels.[17] The motivation here was to investigate differences in the interaction of nanomaterials with vascular cells with a "young" and "aged" phenotype. As a proof of concept, we have selected vascular toxicity as the main readout because it is relatively easy to

quantify; however, cellular NP internalization was also quantified in some experiments. We have used a monoculture of both iPSC-derived ECs either in polystyrene culture dishes (2D) or in Matrigel (3D) to screen, in static conditions. Some of the toxic formulations were further tested in a blood vessel on a chip formed by a co-culture of iPSC-ECs and iPSC-SMCs.

2. Results

Characterization of nanomaterials

We have selected 30 nanomaterials, both organic and inorganic, with different sizes and zeta potentials to evaluate in our vascular screening platform (Table 1). We focused on nanomaterials used for: (i) molecular imaging (NP4), (ii) sunscreen (NP15 and NP16), (iii) antimicrobial applications (NP29, NP9[18] or NP12[19]), (iv) pharmaceutical applications (NP20 and NP21[20], NP24[21], and light-triggerable formulations recently synthesized by us such as NP30, NP23, NP26, NP27, NP18 (all described in reference[22]), NP22[23], NP14[23], and NP25[24]) and (v) reaction catalysis or biomedical applications (NP1, NP2, NP3, NP5, NP6, NP7, NP8, or silica-based NPs such as NP13 and NP28). Many of these NPs may get inside of the human body and interact with blood vessels in the circulation. Dynamic light scattering (DLS) analyses showed that the average sizes of the inorganic nanomaterials suspended in PBS varied between 1 (NP1) and 360 nm (NP29) while for organic nanomaterials varied between 32 (NP10) and 427 nm (NP30) (Figure 2A.1 and 2A.2). Most of the nanomaterials maintained their size after 24 h in suspension with few exceptions (NP8 and NP16 slightly increased their diameters while NP28 decreased significantly their diameters, likely due to a poor initial dispersion of the NPs as shown by TEM analyses, see below). The hydrodynamic diameter of the nanomaterials ranged between 1.1 and 427 nm. Transmission electron microscopy (TEM) analyses were performed to confirm the sizes and shapes of some of the nanomaterials (Figure S1, Supporting Information).

To study the effect of salts and proteins on NP size and stability, the hydrodynamic diameters of NPs (suspended at a concentration of 50 μg/mL) was evaluated by DLS in cell culture media with serum (2% fetal bovine serum (FBS); concentration of serum used to culture ECs) for 24 h (duration of most *in vitro* experiments) (Figure 2A.3 and 2A.4). In cell culture media, with some exceptions (NP12, NP14, NP18, NP29 and NP30 increased their diameters while NP16 and NP17 slightly decreased their diameters), the NPs maintained their diameters for at least 24 h. The hydrodynamic diameter of the NPs ranged between 1.1 and 357 nm. All the NPs showed a negative zeta potential in cell culture medium which indicates that proteins and salts have adsorbed to their surface (Figure 2B). The most negatively charged NP was NP29. Overall, we have selected a library of NPs that are relevant for biomedical and environmental applications. These NPs maintained a reasonable level of stability in cell culture media for at least 24 h.
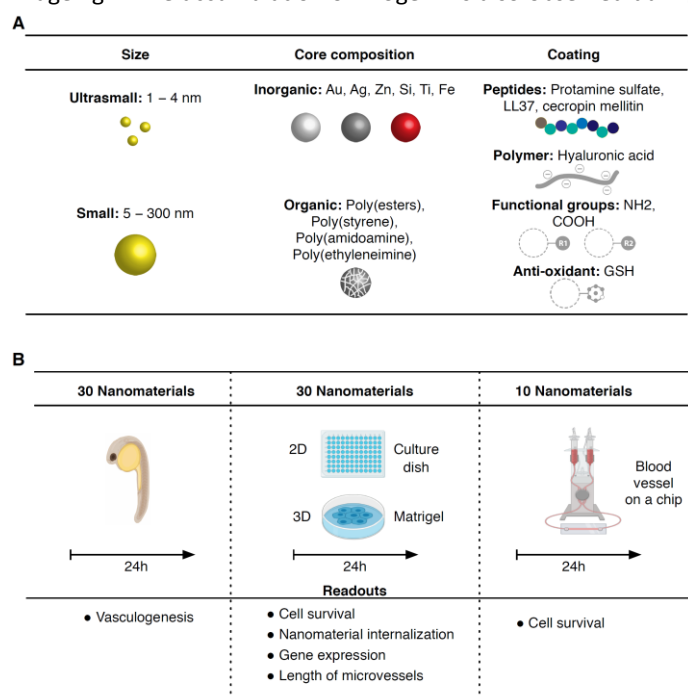
ARTICLE

Table 1 - Summary of the NP sources and properties.

NP Number	Core	Ligand	Size (nm)	Zeta (mV)	Source/Ref.	NP Number	Core	Ligand	Size (nm)	Zeta (mV)	Source/Ref.
NP1	Au	MS	1.4	--	[25]	NP16	TiO2	--	10~30	--	ssnano.com
NP2	Au	GSH	1.5	--	[25]	NP17	PS	COOH	100	--	micromod.de
NP3	Au	HA	5±1[a]	-25±2[a]	N.A.	NP18	C11	--	65±5	14±1	[22]
NP4	SPION	DEX	40	31	biopal.com	NP19	PS	NH2	100	--	micromod.de
NP5	Au	MS	13.9	--		NP20	PLGA	--	170±7	-9±3	[20]
NP6	Au	GSH	12	--		NP21	PLGA-PS	--	218±9	7±2	[20]
NP7	Au	MS	15±1.5	--	[25]	NP22	P1C5	--	350±35	21±2	[23]
NP8	Au	HA	20±3[a]	-26±3[a]	N.A.	NP23	A9	--	265±23	21±2	[22]
NP9	Au	LL37	21±8	15±2	[18]	NP24	PEI:DS	--	91±6	15±3	[21]
NP10	PM	COOH	25	--	micromod.de	NP25	PEI-DMNC:DS	--	108±10	27±2	[24]
NP11	PM	NH2	25	--	micromod.de	NP26	E1	--	330±24	7±1	[22]
NP12	Au	CM	14±1	28±2	[19]	NP27	E2	--	260±18	-2±2	[22]
NP13	SiO2	--	7~14	--	plasmachem.com	NP28	SiO2	--	10~20	--	ssnano.com
NP14	P1C7	--	74±10	19±1	[23]	NP29	Ag	--	<6000	--	sciessent.com
NP15	ZnO	--	10~30	--	ssnano.com	NP30	A1	--	420±14	-1±1	[22]

[a] Determined in water by DLS (*n* = 3). Ligand: MS – Sodium 3-(diphenylphosphino)benzene sulfonate; GSH – Glutathione; HA – Hyaluronic acid; DEX – Dextran; LL37 – Antimicrobial peptide; CM – Cecropin Melittin
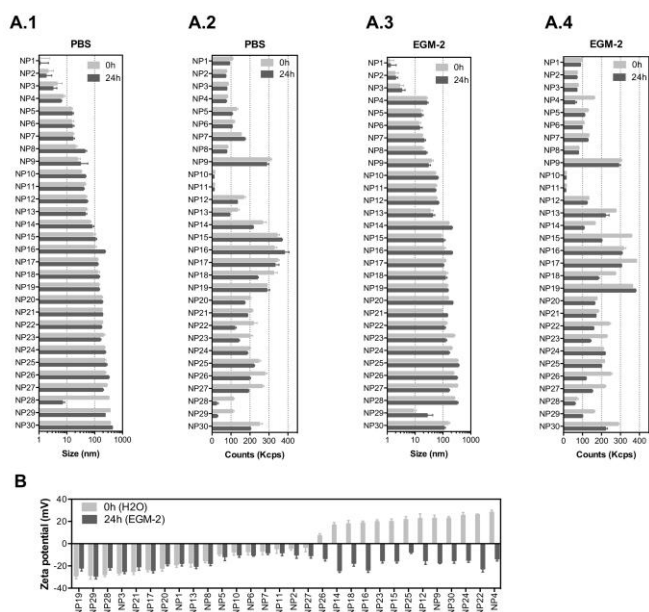

Figure 2 Physicochemical characterization of the NP library. (A) NP size and counts measured by dynamic light scattering at 0 and 24 h in PBS (A.1 and A.2) and EGM-2 medium (A.3 and A.4). (B) Zeta potential of NP library at 0 h (in molecular biology grade water) and 24 h (in EGM-2 medium). After 24 h in EGM-2, the NPs were centrifuged and resuspended in H2O for zeta potential measurements. In A and B, results are expressed as Mean ± SEM (n =3).

Nanomaterial screening in zebrafish

We evaluated the effect of nanomaterials in the vasculogenesis and angiogenesis using the zebrafish transgenic Tg(fli1a:EGFP)[y1] line.[26] In this transgenic, the promoter of the endothelial marker *fli1* drives the expression of EGFP in blood vessels, thus allowing the *in vivo* analysis of the vasculature. In zebrafish embryos, the circulation begins after 24 h-post-fertilization (hpf) in a single vein and a primitive cranial vasculature occurs at this stage.[28] After the formation of this primitive vasculature, the formation of new blood vessels occurs via angiogenesis, being the intersegmental vessels (ISV) of the trunk among the first angiogenic vessels to be formed.[29] The ISV sprout from the dorsal aorta along the somite boundaries, which ultimately interconnect between each other to form the dorsal longitudinal anastomotic vessel (DLAV) (Figure S2A, Supporting Information). Having this is mind, we evaluated the effect of nanomaterials in the vascular development of ISV during the first 24-28 hpf. Fertilized embryos were selected and manually dechorionated to avoid any interference of the chorion in the internalization of the NPs. Indeed, previous studies have demonstrated that the presence of the chorion may affect the toxicity effect of some NPs.[30] For example, Ag NPs caused higher mortality and malformations in embryos without chorion as compared with embryos with chorion at the same concentrations.[30] In our study, the dechorionation caused higher sensitivity of the embryos to their environment, so we used NPs at a concentration of 1 μg/mL. The number of ISV, the average length of the first 10 ISV and the total length of ISV were evaluated (Figure 3 and Figure S2B). Our results showed that some NPs had a negative impact in angiogenesis by decreasing the length of ISVs (NP1, NP3, NP4, NP7, NP8, NP14, NP17, NP18, NP21, NP24, NP25 and NP26) whereas one nanomaterial (NP9) had a positive impact in angiogenesis by increasing the length and number of ISVs (although not statistical significant relatively to control). The pro-angiogenic activity of LL37-Au NPs is aligned

with our previous results showing that these NPs promoted neovascularization in a wound healing animal model.[18]
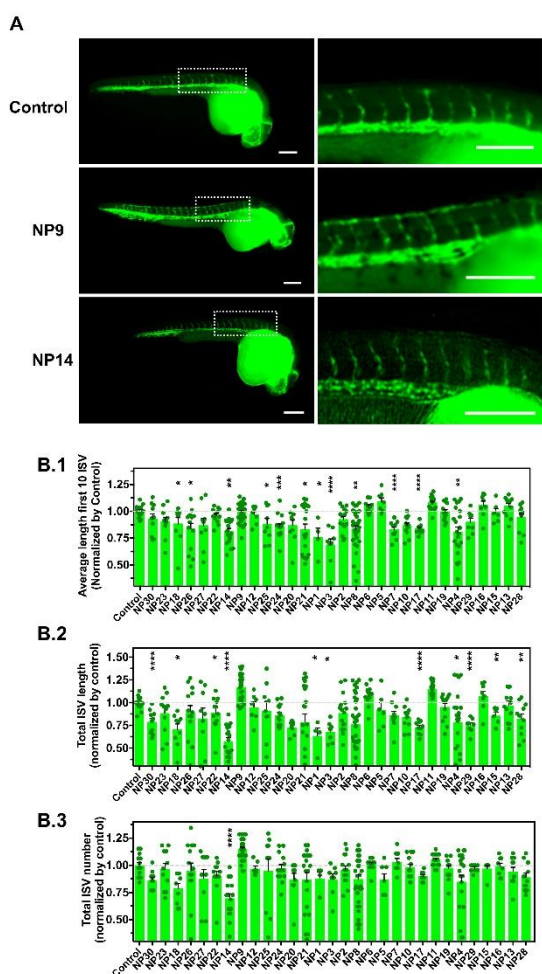

Figure 3 - Impact of nanomaterials in the embryonic vascular development of zebrafish embryos. (**A**) Representative fluorescence microscopy images (all embryo and magnification of the first 10 ISV´s) of zebrafish embryos with ~28 hpf in control conditions (vehicle) and after 24 h treatment with NP9 and NP14. Scale bar is 200 μm. (**B.1**) Impact of 24 h incubation of nanomaterials in the average length of the first 10 ISV of zebrafish embryos with ~28 hpf. (**B.2**) Impact of 24 h incubation of nanomaterials in the total ISV length of zebrafish embryos with ~28 hpf. (**B.3**). Impact of 24 h incubation of nanomaterials in the total number of ISV of zebrafish embryos with ~28 hpf. In B.1, B.2 and B.3, results are Mean ± SEM (n=6-24) and statistical analyses were performed by an unpaired t-test. *, **, **** denotes statistical significance ($P<0.05$; $P<0.01$; $P<0.0001$) relative to control.

Development of a vascular screening platform based on iPSC-derived vascular cells: derivation of endothelial cells from hiPSCs

iPSC lines were differentiated into ECs according to a protocol previously reported by us[13] (Figure 4A). Undifferentiated cells were cultured in chemically defined medium supplemented with BMP4 and FGF-basic for 5 days to generate mesoderm progenitor cells followed by their differentiation into endothelial progenitor cells (PECAM1+ cells) in media containing VEGF and Tβ4 for an additional 5 days. PECAM1+ cells were then selected by magnetic-activated cell sorting and cultured for up to 7 passages in endothelial medium supplemented with

VEGF165 and TGF-β inhibitor (SB431542). Gene expression analysis in cells differentiated for 7 passages (between 24 and 28 days after cell seeding) indicated that both N-iPSC ECs (from non-disease cord blood cells) and HGPS-iPSC ECs expressed EC markers such as *PECAM1*, *CDH5, KDR* and *vWF* as human umbilical artery ECs (HUAECs), although with some fluctuations in the expression of these markers (Figure 4B). In general, the mRNA levels of the EC markers were higher in HGPS-iPSC ECs than in N-iPSC ECs. N-iPSC-derived or HGPS-iPSC-derived PECAM1+ cells cultured for 7 passages expressed high levels of EC markers such as PECAM1 [by immunocytochemistry (Figure 4C) and flow cytometry (Figure S3A)], VE-cadherin and ZO-1 at cell-cell contacts (Figure 4C) as well as endoglin (CD105). In contrast to N-iPSC ECs, HGPS-iPSC ECs expressed Progerin, the truncated form of Lamin A. Indeed, 61±18% (n=3) of HGPS-iPSC ECs had accumulation of Progerin, as quantified by immunofluorescence. The presence of nuclear blebs (characteristic of progeria cells) was also observed by immunostaining of Lamin A/C (inset in Figure 4C). At the functional level, both N-iPSC ECs[13] and HGPS-iPSC ECs responded to pro-inflammatory stimuli such as TNF-α for 24 h leading to an increase in the expression of adhesion molecules which then mediated the adhesion of monocytes (Figure S3C, hiPSC lines). The derived cells expressed EC markers at gene and protein levels and were functional.
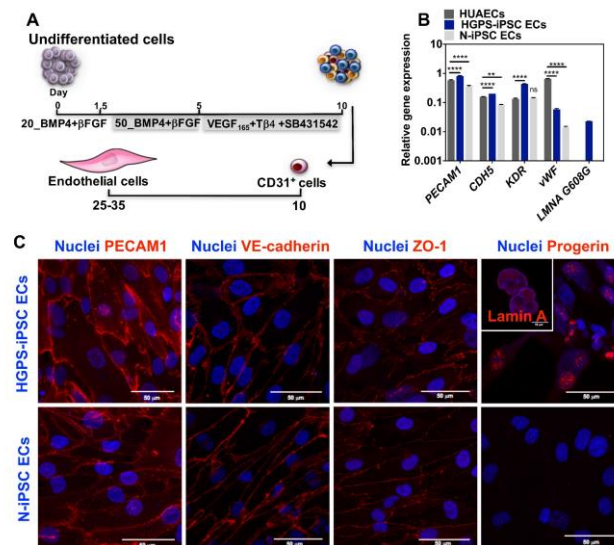

Figure 4 - Characterization of iPSC-ECs. (**A**) Protocol for the differentiation of N-iPSCs and HGPS-iPSCs into EC cells. Undifferentiated iPSCs were transferred to petri dishes coated with fibronectin and were cultured in differentiation medium for a period of 10 days (see methods section for more details), after which the PECAM1+ cells were selected by magnetic-activated cell sorting and cultured with full culture medium supplemented with VEGF165 and SB431542 for 7 passages (~25 days) with medium changed every 2-3 days. (**B**) qRT-PCR analyses for the expression of endothelial and progeria genes. Expression of EC (*PECAM1*, *CDH5*, *KDR* and *vWF*) and progeria (progerin which is encoded by *LMNA G608G* gene) markers in HGPS-iPSC and N-iPSCs at passage 7. Human umbilical aortic endothelial cells (HUAECs) were used as controls. Results are Mean ± SEM (n=3). **,**** denotes statistical significance ($P<0.01$, $P<0.0001$) normalized by the housekeeping gene (GAPDH). Statistical analyses were performed by an unpaired t-test. (**C**) Immunofluorescence analysis performed on HGPS-iPSC ECs and N-iPSC ECs at passage 7 for EC (PECAM1, VE-cadherin, ZO-1) and progeria (progerin) markers. Cell nuclei was labelled with DAPI (blue). Scale bar is 50 μm.

Vascular screening of NPs in a 2D model

The impact of the nanomaterial library was evaluated in ECs derived from N-iPSCs or HGPS-iPSCs cultured in static conditions. Cells were cultured for 24 h, washed and then exposed for 24 h to distinct concentrations of the nanomaterials (6, 12.5, 25 and 50 µg/mL) (Figure 5A). The effect of the NPs was quantified by two tests: (i) cell metabolism through the measurement of mitochondrial activity by a PrestoBlue assay and (ii) cell necrosis by counting cell nuclei using a Hoechst 33342/propidium iodide (PI) staining (Hoechst to quantify the total number of cells; PI to quantify the dead cells). Because some NPs may interfere with PrestoBlue assay,[31] cells after being incubated with NPs for 24 h were washed 3 times with PBS before incubating with PrestoBlue. These washing steps (which were not necessary and thus not performed in the Hoechst 33342/PI assay) likely induced higher cell detachment/loss, especially when NPs cause some toxicity, which may lead to an apparent low mitochondrial activity. This might be the reason why the PrestoBlue results appeared to show more toxic effect for some NPs then the corresponding Hoechst 33342/PI assay. Therefore, primarily, we have used Hoechst /PI staining to compare all the experimental groups. From the thirty nanomaterials tested, 7 induced significant toxicity (> 60% at 50 µg/mL; based on PI staining) towards both hPSC-derived ECs tested (i.e., NP1, NP3, NP14, NP15, NP18, NP22 and NP30) whereas 2 nanomaterials (NP25 and NP28) induced significant toxicity only towards N-iPS ECs (Figure 5B-5E). The high toxicity observed for NP1 and NP3 NPs (i.e., ultrasmall Au NPs) is in agreement with previous results obtained in HeLa cells, with a reported IC50 of about 50 µM.[25, 32] The toxicity of NP15 (ZnO) is in line with the toxic profile observed previously in human aortic ECs (>50% for 4 to 24 h incubation at 50 µg/mL),[33, 34] human cardiac microvascular ECs (>60% for 12 to 24 h incubation at 50 µg/mL)[35] and in human umbilical vein ECs (HUVECs) (>75% for 24 h incubation at 32 µg/mL).[36, 37] Regarding NP28, the results are also in accordance with those reported in the literature for HUVECs exposed for 24 h, with toxicities ranging from 20 to 60% for 50 and 75 µg/mL SiO$_2$ concentrations, respectively.[38]

NPs showed a differential toxic effect against both types of ECs. HGPS-iPSC ECs were more sensitive to NP13, NP18, NP22, NP26 and NP29 NPs as compared to N-iPSC ECs (Figure 5B-5E). However, NP3, NP7, NP24, NP25, and NP28 were more toxic for N-iPSC derived ECs than HGPS-iPSC ECs.

To investigate whether the nanomaterial toxicity correlates with its capacity to be internalized by ECs, we performed inductively coupled plasma mass spectrometry measurements (ICP-MS) on N-iPSC ECs and HGPS-iPSC ECs exposed to 11 different nanomaterials (25 µg/mL) for 24 h (Figure 5F). The concentration of NPs was selected based in a compromise between cell death and NP quantification before cell death. For one of the nanomaterials tested (NP1), the accumulation was evaluated after 4 h incubation with cells, because of the high toxicity observed after 24 h incubation. Overall, our results indicate that the toxicity of the NPs was not dependent on the

concentration internalized by the cells. For example, NP24, NP25 and NP30 had similar ranges of cytotoxicity (Figure 5E.1) against N-iPSC ECs but significant differences in NP uptake (Figure 5F). On the other hand, the cellular uptake of NP1 and NP7 was very low compared to other NP formulations;
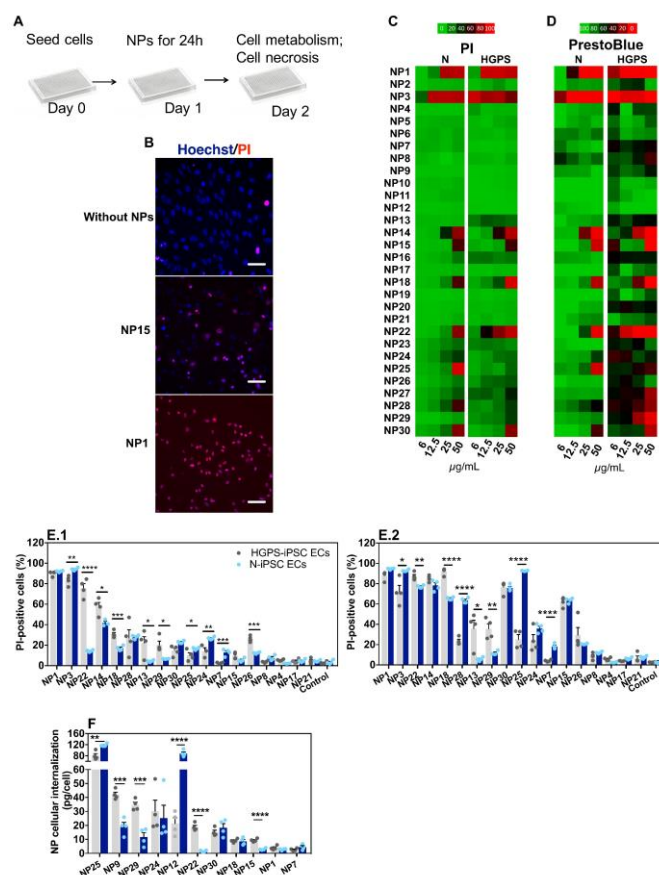

Figure 5 - Impact of nanomaterials in iPSC-ECs cultured in 2D. (**A**) Schematic representation of the protocol used. Cells were seeded at density of 1×10^5 cells/cm^2 and were allowed to rest for 24 h, after which NPs were added in fresh medium at concentrations between 6 and 50 µg/mL for a 24 h period. Cell viability was evaluated by Hoechst 33342/PI staining while cell metabolism was quantified by PrestoBlue assay. (**B**) Representative images of Hoechst 33342/PI staining for N-iPSC ECs with (NP1 or NP15, both at 50 µg/mL) or without exposure to NPs for 24 h. Scale bar is 50 µm. (**C, D**) Heat maps of NPs toxicity based on Hoechst 33342/PI staining (**C**) and PrestoBlue assay (**D**; normalized by control cells, without NPs). (**E**) Toxicity observed by PI staining in N-iPSC ECs and HGPS-iPSC ECs exposed to NPs at 25 µg/mL (E.1) and 50 µg/mL (E.2). Results are Mean ± SEM (n =4). *, **, **** denotes statistical significance (*P<0.05, P<0.01, P<0.0001*). (**F**) ICP-MS analyses in N-iPSC ECs and HGPS-iPSC ECs after being exposed to NPs for 24 h (except for NP1 which was 4 h incubation). Results are Mean ± SEM (n =4). **, ***,**** denotes statistical significance (*P<0.01, P<0.001, P<0.0001*). In E and F, the statistical analyses were performed by an unpaired t-test.

however, they exerted a higher cytotoxic effect against ECs. In addition, one (NP12) showed high cellular internalization (Figure 5F), mostly by N-iPSC ECs, without showing measurable toxicity (Figure 5C). Interestingly, some nanomaterials were more internalized by HGPS-iPSC ECs than N-iPSC ECs and this is surprising taking into account that HGPS-iPSC ECs showed lower cell doublings than N-iPSC ECs (Figure S3B, Supporting Information).

Overall, our results indicate that: (i) NPs showed a differential toxic effect against both types of ECs and (ii) there is not a direct

correlation between the concentration of NPs internalized by cells and the observed toxicity *in vitro* under static conditions. Regarding this last point, some NPs showed high internalization efficiency without causing any toxic effect on cells, whereas others caused high toxicity with very low internalization efficiency.

Vascular screening of NPs in a 3D model

The vascular impact of the NPs was then screened in a Matrigel assay[39] comprising the formation of microvessels with a patent lumen, as previously demonstrated by us.[12] The optimization of the assay (e.g. cell exposure time to nanomaterials, concentration of nanomaterials, type of readouts) was carried out with somatic ECs (human umbilical arterial ECs) (Figure S4, Supporting Information). Cells were cultured on top of Matrigel in the presence of NPs for 24 or 48 h after which EC viability and tube length was measured. The option of mixing the NPs during the formation of microvessels, and not after, was inspired by the *in vivo* strategy described below in zebrafish embryos in which the effect of the NPs was evaluated during, and not after, embryonic vasculature formation. Our results indicate that cells exposed to NP1 at 1 μg/mL for 24 h had no significant effect while at 12.5 μg/mL showed approximately 12% and 14% of apoptosis and necrosis, respectively, and were unable to form vascular microvessels in Matrigel (cells showed clear altered morphology) (Figure S4, Supporting Information). Therefore, for the screening assay in Matrigel we have used N-iPSC-ECs, a concentration of nanomaterials of 12.5 μg/mL and we evaluated the length of the microvessels after 24 h (Figure 6A). Interestingly, only three formulations could affect negatively microvessel formation, specifically NP1, NP3 and NP29 that reduced or even abolished the formation of microvessels (Figure 6B.1). Interestingly, NP9 enhanced angiogenesis, as LL37 peptide is a recognized pro-angiogenic peptide.[18]

Next, to compare the vascular response in 3D versus 2D (see section above), we have mixed NP formulations (at a concentration of 25 μg/mL) with N-iPSC ECs or HGPS-iPSC ECs, cultured the cells in Matrigel for 24 h and measured cell toxicity by Hoechst/PI staining. We have selected 6 NP formulations for these analyses including NP1, NP3, NP4, NP14, NP15 and NP29 since they showed cytotoxicity in a 2D model (Figure 5C). The toxicity level (based on PI staining) of NP1 and NP3 was lower than the one observed in a 2D model (NP1: 60 *vs* 90%; NP3: 40 *vs* 90%, all based in N-iPSC ECs); however, it was higher for NP29 (N-iPSC ECs: 20 *vs* 10%; HGPS-iPSC ECs: 40 vs 20%). Our results further showed differences in NP toxicity against N-iPSC ECs and HGPS-iPSC ECs (Figure 6C). For example, NP4 and NP14 induced higher toxicity towards N-iPSC ECs than HGPS-iPSC ECs. In contrast, NP29 induced higher toxicity towards HGPS-iPSC ECs than N-iPSC ECs, similar to the results obtained with the 2D model (Figure 5).

Previous studies have shown that the accumulation of Progerin in ECs induced a pro-inflammatory program of EC activation characterized by an overexpression of leukocyte adhesion molecules (VCAM1, E-selectin)[40] and pro-inflammatory cytokines (IL8)[40] and a downregulation of the transcription

factor Kruppel-like factor (KLF2)[40] which regulates EC pro-inflammatory activation, but also a decrease in the anti-oxidative stress response program characterized by an impaired transcriptional activity of the transcription factor NRF2.[41] Indeed, HGPS-iPSC ECs have higher reactive oxidative species levels than N-iPSC ECs (Figure S5, Supporting Information). To identify the mechanism behind the differential toxicity of NPs against N-iPSC ECs and HGPS-iPSC ECs, we evaluated the expression of genes involved in oxidative stress (*NRF2*), inflammation (*SELE*, *ICAM1, VCAM1* and *IL-8*) and endothelial homeostasis (*KLF2, VEGF*) in cells exposed to NP14 and NP29 (both at 25 μg/mL) for 24 h (Figure 6D). In the absence of NPs, HGPS-iPSC ECs showed higher expression of inflammatory and oxidative stress but lower *KLF2* mRNA transcripts than N-iPSC ECs. After exposure to NPs, the inflammatory response of both cells was significantly different: only N-iPSC ECs showed a
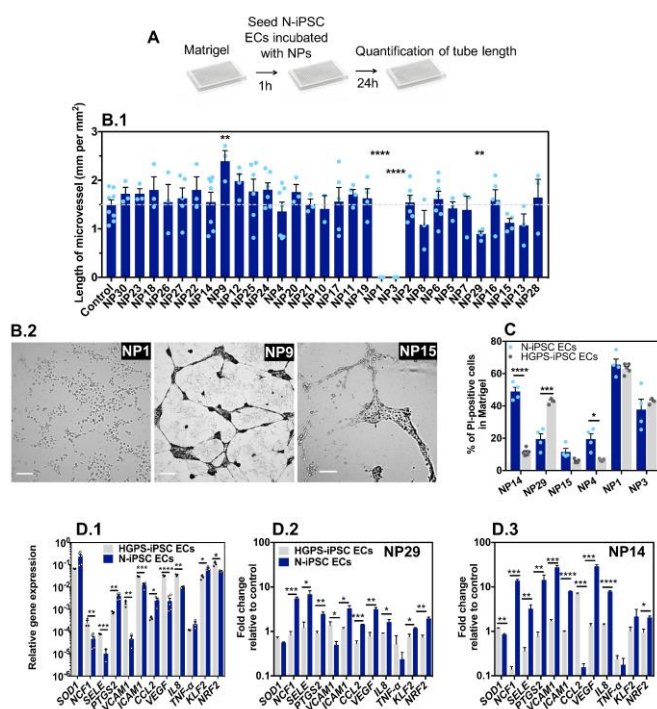

Figure 6 - Impact of nanomaterials in iPSC-ECs cultured in 3D. (A) Schematic representation of the protocol to evaluate the effect of NPs in the formation of capillary-like networks by iPSC-ECs on Matrigel. Cells were seeded on top of Matrigel at a density of 2×10³ cells/well together with NPs (12.5 μg/mL) for 24 h, after which cell viability and tube formation was analyzed. **(B.1)** Impact of NP library in the length of microvessels formed by N-iPSC ECs. Results are Average ± SEM (n=4). **, **** denotes statistical significance (*P<0.01, P<0.0001, respectively*) relatively to control. **(B.2)** Representative images of capillary-like networks formed in Matrigel by N-iPSC ECs treated for 24 h with 12.5 μg/mL of NP1, NP9 or without NPs (Control). Scale bar is 200 μm. **(C)** Toxicity was measured by Hoechst 33342/PI staining at 24 h, in HGPS-iPSC ECs or N-iPSC ECs cultured in the presence of NP1, NP3, NP4, NP14, NP15 and NP29 in Matrigel at 25 μg/mL. *, ***,**** denotes statistical significance (*P<0.05, P<0.001, P<0.0001*). **(D)** Relative gene expression of genes involved in oxidative stress (*NRF2*), inflammation (*ICAM1, SELE, VCAM1* and *IL8*) and endothelial homeostasis (*KLF2, VEGF*) in N-iPSC ECs and HGPS-iPSC ECs before (**D.1**) and after exposure to 25 μg/mL of NP29 (**D.2**) or NP14 (**D.3**). *, **,*** denotes statistical significance (*P<0.05, P<0.01, P<0.001*). In B.1, C and D, the statistical analyses were performed by an unpaired t-test.

significant up-regulation of pro-inflammatory mRNA and the response seemed higher for NP14 than NP29. Moreover, N-iPSC ECs, but not HGPS-iPSC ECs, showed an upregulation of mRNA of *NRF2* gene that encodes nuclear factor erythroid 2-related factor involved in the cellular antioxidant response. Altogether, our results indicate that: (i) a small number of NPs (3 out of 30) interfered with microvessel formation in Matrigel at the concentrations tested (12.5 μg/mL); (ii) the Matrigel assay showed differences in the vascular toxicity profile (evaluated by PI staining) of NPs relative to the 2D model, but in both cases the importance of EC background was critical for the biological response; (iii) the differential biological response of N-iPSC ECs and HGPS-iPSC ECs to NPs involved differential regulation of genes related with inflammation and oxidative stress.

Screening of NPs in a blood vessel on a chip

The vascular models described above have several limitations, including the fact that they are not perfused and do not take into account the heterotypic interactions between ECs and SMCs. Cells exposed to flow change their morphology and more importantly they express a layer of proteins, glycoproteins, glycolipids, proteoglycans and glycosaminoglycans called glycocalyx.[42] The glycocalyx is involved in several functions, such as regulation of vascular permeability, acting as a selective barrier to macromolecules (based on size and charge), as well as a mechanosensor of fluid shear stress. Thus, we decided to prepare a blood vessel on a chip to screen nano-bio interactions. In general, these chips have only one layer of endothelial cells to evaluate nano-bio interactions.[43] Here, we have successfully developed a chip with two cell monolayers of SMCs and ECs. The vessel was perfused with medium, at shear rates similar to *in vivo*, and the EC monolayer was able to secrete a functional glycocalyx layer on top. For this purpose, SMCs (for initial studies we have used somatic cells) were cultured in a microfluidic chamber for 12 h to form a monolayer followed by the plating of ECs on top of SMCs for 4 h and finally by the perfusion of both cells for 5 days (Figure S6, Supporting Information). Under these conditions, SMCs were in the outer part of the vessel while ECs remained in the luminal side (Figure S6A and S6B, Supporting Information). Interestingly, ECs co-cultured with SMCs under flow conditions showed higher levels of glycocalyx than ECs alone cultured under flow conditions (Figure S7A, Supporting Information). To verify that the glycocalyx was indeed located in the luminal side of ECs, we have used GFP-expressing ECs which were co-cultured with SMCs for 5 days under flow as previously described (Figure S7B and S7C, Supporting Information). As expected, the layer of glycocalyx was located on top of the EC layer in the luminal side, showing the polarization of the glycocalyx. The formation of the glycocalyx was also demonstrated by an EC uptake assay of DiI-LDL (Figure S7D, Supporting Information). In this case, cells cultured under flow conditions for 5 days had lower uptake of Dil-LDL than cells cultured for 5 days and exposed to heparinase III to remove the heparin sulfate in glycocalyx.
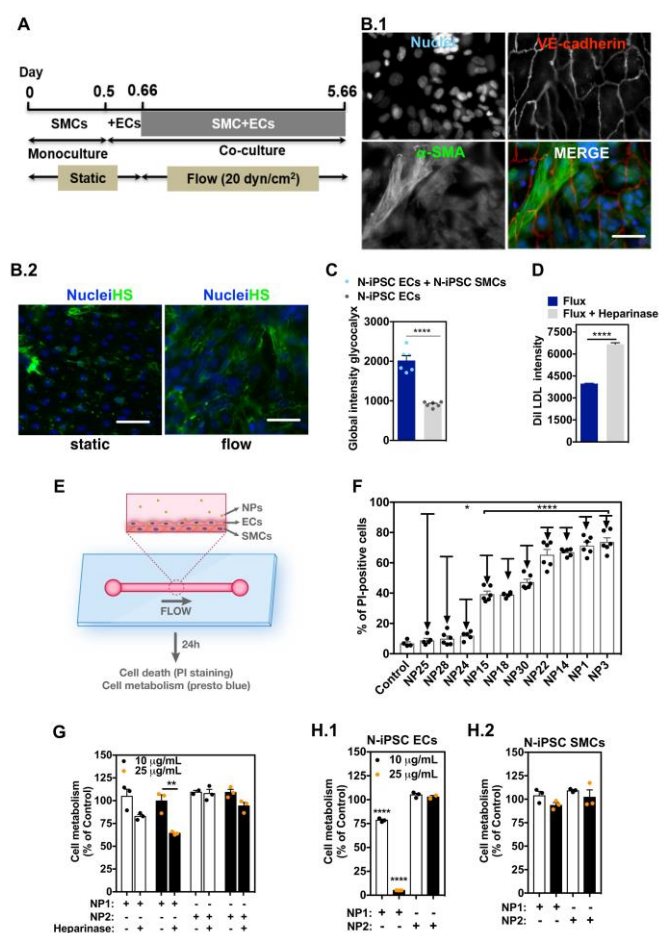

Figure 7 - Impact of nanomaterials in a blood vessel on a chip composed by iPSC-ECs and iPSC-SMCs. (**A**) Protocol to generate a blood vessel on a chip. A suspension of SMCs (4.1×10^4 cells/cm^2) was applied in each channel of an Ibidi μ-Slide VI ^{0,4} plate. SMCs were maintained in static conditions for 12 h, after which a suspension of ECs (12.5×10^4 cells/cm^2) was applied on top of SMCs and the co-culture was maintained in static conditions for 4 h, after which cells were perfused with EGM-2 medium at 20 dyn/cm^2 for 5 days. (**B**) Immunofluorescence analyses performed on a co-culture of N-iPSC SMCs and N-iPSC ECs for: SMC (α-SMA), EC (VE-cadherin) (**B1**) and glycocalyx (heparan sulfate) (**B2**) markers. Scale bar is 50 μm. (**C**) Heparan sulfate intensity in a co-culture of N-iPSC SMC and N-iPSC EC cells *vs* monoculture of N-iPSC ECs after 5 days under arterial flow conditions (20 dyn/cm^2). **** denotes statistical significance ($P<0.0001$). (**D**) Effect of glycocalyx impairment (by heparinase III treatment) in the uptake of DiI-LDL by N-iPSC ECs after 5 days in co-culture with N-iPSC SMCs under arterial flow conditions (20 dyn/cm^2). **** denotes statistical significance ($P<0.0001$). In C and D, the statistical analyses were performed by an unpaired t-test. (**E**) Schematic representation of the protocol. Cells (co-culture of N-iPSC SMCs and N-iPSC ECs) were cultured for 5 days in arterial flow conditions (20 dyn/cm^2), after which NPs were incubated for 24 h and characterized for cell metabolism and death. (**F**) Cell viability after 24 h incubation in flow conditions measured by Hoechst 33342/PI staining. Arrows show the difference in toxicity between static (monoculture of N-iPSC ECs) and flow conditions (co-culture N-iPSC SMCs and N-iPSC ECs) for the same NPs. Results are Mean ± SEM (n=4-6). *, **** denote statistical significance ($P<0.05$, $P<0.0001$) against control (cells without NPs). (**G**) Effect of the removal of endothelial glycocalyx, by heparinase III treatment, in the metabolism of N-iPSC ECs and N-iPSC SMCs cultured in microfluidic chip for 24 h with NP1 or NP2. ** denotes statistical significance ($P<0.01$) against control (cells without NPs). (**H.1**) Cell metabolism of N-iPSC ECs after 24 h incubation with NP1 or NP2 under arterial flow conditions. **** denotes statistical significance ($P<0.0001$) against control (cells without NPs). (**H.2**) Cell metabolism of N-iPSC SMCs after 24 h incubation with NP1 or NP2 under arterial flow conditions. In F, G and H, results are Mean ± SEM (n=3) and statistical analyses were performed by an unpaired t-test.

In order to verify the effect of flux in the formation of glycocalyx, SMC and ECs were co-cultured as previously described and the heparan sulfate intensity was quantified at different time points (Figure S8A, Supporting Information). The amount of heparan sulfate increased more than 2.5-fold up to 5 days in flow, at 20 dyn/cm^2 (Figure S8B and S8C, Supporting Information). The recovery of heparan sulfate was also evaluated. Cells cultured under flow for 5 days were treated with heparinase III to degrade the heparan sulfate, and its recovery was followed over time (Figure S8D). The kinetics of the recovery was similar to the one observed for the heparan sulfate formation induced by the shear stress. Therefore, for subsequent experiments with iPSC-derived cells, they were co-cultured for 5 days at 20 dyn/cm^2. We performed experiments with N-iPSC SMCs and N-iPSC ECs (Figure 7A) but not HGPS-iPSC derived cells because the HGPS-iPSC SMCs were sensitive to flow and detached overtime.[44] N-iPSC SMCs obtained using protocols previously published by us[45] were cultured in a microfluidic chamber followed by the culture of N-iPSC ECs on top of the SMCs (Figure 7B). Cells were then cultured under flow conditions (20 dyn/cm^2) for 5 days. Under these conditions, N-iPSC SMCs were located in the outer part of the blood vessel and positively stained for α-smooth muscle actin (α-SMA) whereas the iPSC-ECs, which were located in the inner part of the blood vessel, were positively stained for VE-cadherin (Figure 7B.1). As expected, ECs expressed glycocalyx being the expression higher in flow than in static conditions (Figure 7B.2) and in co-culture with SMCs *versus* ECs alone (Figure 7C). Moreover, the enzymatic removal of heparan sulfate by heparinase in vascular cells cultured under flow conditions for 5 days allowed higher accumulation of Dil LDL (Figure 7D) than cells without enzymatic treatment. Altogether, we have developed a blood vessel on a chip from ECs and SMCs derived from iPSCs. ECs co-cultured with SMCs under flow conditions expressed higher levels of heparan sulfate than ECs cultured in static conditions and thus represent a better match to the *in vivo* blood vessel physiology.

Next, we have tested the 10 NPs identified in previous vascular models with higher cytotoxicity effect in a blood vessel on a chip (Figure 7E). In this model, we used ECs and SMCs derived from N-iPSCs. Ten NPs were exposed for 24 h under flow conditions to the blood vessel on a chip. For two of the formulations (NP15 and NP25) we have also quantified the cellular internalization of the NPs by ICP-MS analyses. The results show that NP internalization was 34.6 pg/cell and 1.1 pg/cell (assuming that all the NPs were taken up by ECs alone) of NP15 and NP25, respectively, which means approximately 3-fold lower than in static conditions (Figure S9, Supporting Information). Interestingly, all the NPs tested showed lower toxicity than in static conditions against N-iPSC ECs (Figure 7F). The decrease in toxicity may be explained by the protective role of glycocalyx expressed in the blood vessel on a chip. To demonstrate this hypothesis, the toxicity of NP1 and NP2 was evaluated in 3 different models: (i) a co-culture of N-iPSC SMCs and N-iPSC ECs (Figure 7G), (ii) a monoculture of N-iPSC ECs (Figure 7H.1) and (iii) a monoculture of N-iPSC SMCs (Figure 7H.2). As shown before (Figure 7C and S7A, Supporting Information), a co-culture of SMCs and ECs lead to an increase of the production

of the glycocalyx layer showed by a significant increase in intensity of heparan sulfate, one important and main component of the glycocalyx. Our results showed that when ECs had this protective glycocalyx layer the toxicity of NP1 was considerably lower than in cells without this layer (Figure 7G). In addition, and when the glycocalyx layer was impaired, either by enzymatic degradation (Figure 7G) or by using the monoculture cell model of ECs (that produces less glycocalyx; Figure 7H.1), the toxicity was higher relative to cells with glycocalyx layer. iPS-SMCs showed no toxicity towards these NPs at the concentrations tested (Figure 7H.2). Therefore, the presence of a glycocalyx layer influenced the impact of NPs in ECs and might explain differences in the toxicity of nanomaterials in static *vs* flow conditions.

Overall, our results indicate that most of the nanomaterials that had a negative impact in the angiogenesis of blood vessels in the transgenic zebrafish model showed vascular toxicity in the 2D and 3D models but with differences according to the type of vascular cells and their organizational complexity. In addition, the toxicity of the tested NPs was lower in the blood vessel on a chip than in the 2D model. The results further indicate that the decrease in the NP toxicity, at least in part, was mediated by the expression of a protective glycocalyx layer in ECs cultured in the blood vessel on a chip.

3. Discussion

The current work describes a platform to study the bioactivity/toxicity of nanomaterials based on vascular cells derived from hiPSCs which were cultured in 3 different platforms with increasing level of complexity: (i) monoculture in poly(styrene) (named as "2D"); (ii) monoculture in Matrigel (named as "3D") and (iii) co-culture (both ECs and SMCs) under flow conditions (named as "blood vessel on a chip"). These 3 platforms captured different aspects of the impact of the nanomaterials and the results were validated in zebrafish embryos, more specifically, in the capacity of the NPs to interfere with embryonic vasculogenesis. The 2D model is the most suitable model for high-throughput screening; however, it does not recapitulate the three-dimensional organization of the blood vessel as well as the dynamic environment of the bloodstream which may induce phenotype alterations in ECs (e.g. absence of glycocalyx expression) and NPs may deposit at higher levels onto the cells which increases NP uptake. The 3D model is suitable to reproduce the geometry of the blood vessel *in vitro* since ECs associate into 3D tubes with lumen formation;[12, 39] however, as the 2D model, it does not take in account the complexity of the blood vessel neither the effect of flow. The blood vessel on a chip is suitable to reproduce the complexity (as it includes ECs and SMCs) and flow culture conditions as observed in the *in vivo* blood vessels; however, it is complex for the use in high-throughput screening. Our results indicate that the 3 platforms were able to identify, at different extents, the NPs that showed toxicity against zebrafish embryos. From the 18 NP formulations that interfered with the vasculogenesis process in zebrafish embryos (Figure 3), 15 NP

formulations have been identified by the *in vitro* models (2D and 3D models; the number of PI+ cells was above 20%), being their toxicity level dependent on the hiPSC-EC type. Some of the formulations were also tested in a blood vessel on a chip and the results further confirmed their toxicity; however, in general, at lower intensity. Table S1 (Supporting information) summarizes the main findings obtained among the four systems as well as rodent data found in the literature.

Previous studies have used 2D models based in somatic ECs, but not ECs derived from hiPSCs generated from different individuals, to screen multiple NP formulations [46]. In addition, hiPSC-ECs have been used to screen small molecules [12] but not nanomaterials. The use of hiPSCs enables the *in vitro* modelling of different individuals with or without diseases. The development of iPSC technology allows the access of virtually unlimited number of cells from any individual which can then be differentiated into any kind of cells and be used for high-throughput screening studies. This technology has allowed, for instance, the screening of large libraries of small compounds to find hits that rescue genetic diseases [47, 48] or interfere with human development.[12] We have used hiPSCs as a source of ECs to study nanomaterial interactions which has not yet been investigated. We have studied the impact of nanomaterials in hiPSC-ECs having an embryonic (N-iPSC ECs)[12] and an aged phenotype (HGPS-iPSC ECs), as confirmed by the accumulation of progerin and the existence of dysmorphic nuclei in the latter. The selection of HGPS-iPSC ECs in the context of this work was to investigate the biological response of aged cells to NPs, which is a topic that remains largely unexplored.

Our results indicate that HGPS-iPSC ECs and N-iPSC ECs had differential toxicity profiles against NPs, both in 2D and 3D models. The ultrasmall NP1 and NP3 showed to be the most toxic of all NPs of the library for both types of ECs, even for concentrations at 6 μg/mL (2D model); five NPs (NP14, NP15, NP18, NP22 and NP30) showed toxicity levels higher than 60% (measured by a PI assay) for both EC-derived cells; three NPs (2D system: NP25 and NP28; 3D system: NP14) showed higher toxicity against N-iPSC ECs rather than HGPS-iPSC ECs; one NP formulation (NP29) showed higher toxicity (3-fold) for HGPS-iPSC ECs than for N-iPSC ECs. The vascular toxicity observed for some NPs in the 2D model are in good accordance to the reported in the literature using somatic cells. For example, NP1 and NP3 showed high toxicity against HeLa cells.[32] Zinc oxide NPs were observed to be toxic (>50%) at 50 μg/mL in human aortic ECs,[34] human cardiac microvascular ECs[35] and in HUVECs;[36, 37] all these results are in good accordance with the 60% toxicity observed in our study for EC derived from iPSC. SiO$_2$ NPs also have been reported to induce toxicities from 20 to 60% in HUVECs for NP concentrations between 50 and 75 μg/mL[38] while Ag NPs have been reported to induce toxicity in rat brain microvessel ECs[49] and to demonstrate anti-angiogenic properties[50]. It is possible that the higher toxicity of Ag NPs against HGPS-iPSC ECs, as compared to N-iPSC ECs, is related to a decrease in the antioxidative stress response program in HGPS-iPSC ECs. It is known that Ag NPs induce cytotoxicity through oxidative stress, leading to the production of reactive oxygen species (ROS) in their surface or though the direct interaction with cell mitochondria.[51] On the other hand, the nuclear accumulation of progerin impairs the transcriptional activation of NRF2, due to the physical interaction of both proteins, which reduces the anti-oxidative stress program of HGPS cells.[41] Therefore, it is expected that HGPS-iPSC ECs are more sensitive to NPs that induce toxicity by oxidative stress such as Ag NPs. In contrast, the higher toxicity of NP14 against N-iPSC ECs as compared to HGPS-iPSC ECs may be related to the differential inflammatory program between cells. Our results show that HGPS-iPSCs have a pro-inflammatory program before NP exposure, characterized by higher levels of *VCAM1, SELE, IL8* and *ICAM1* mRNA transcripts as compared to N-iPSC ECs. It is possible that the pro-inflammatory status of HGPS-iPSC ECs make these cells less sensitive to inflammatory cytokines as N-iPSC ECs. Indeed, the pro-inflammatory program of HGPS-iPSC ECs is not significantly affected after exposure to NPs while the opposite was observed in N-iPSC ECs.

The EC response to NPs is largely influenced by the flow shear stress and the interaction with SMCs. EC genotype/phenotype as well as endocytic capacity are influenced by flow shear stress. For example, ECs cultured under increased shear stress have decreased oxidative stress and inflammation[52] and showed differential NP uptake as compared to ECs cultured under static conditions.[43, 53] Importantly, EC response to flow shear stress is influenced by the neighbouring SMCs.[54, 55] Although *in vitro* co-culture systems of ECs and SMCs under flow conditions have been established for somatic EC and SMCs,[54, 55] the generation of co-culture systems with hiPSC-derived vascular cells remains unexplored. The model developed in the current work allows the performance of assays at arterial conditions by submitting cells to shear stresses of 20 dyn/cm^2. In this model, cells aligned parallel to the flow direction, and ECs produced a glycocalyx (a glycoprotein-polysaccharide meshwork) layer in the apical region as it occurs *in vivo*. Previous studies have shown that glycocalyx influences NP uptake by somatic ECs.[56, 57] Our results showed that NP toxicity against ECs is significantly lower in cells cultured under flow conditions and in co-culture with SMCs. Our results further showed that glycocalyx mediated, at least in part, the reduction in NP internalization since the degradation of glycocalyx by heparinase significantly reduced cell metabolism/viability.

In many cases, the impact of nanomaterials is screened in rodents;[4-6] however, these experiments are expensive, time consuming and low throughput. Zebrafish embryos can be used to investigate vascular toxicity of NPs because they are relatively cheap, the developmental processes are well studied and the toxicity of the NPs can be monitored in real time using transgenic lines with fluorescent markers.[58, 59] Therefore, in the current work, zebrafish embryos were used to validate the toxicity profile of the NP library evaluated in the *in vitro* tests. Because some NPs are trapped by the chorion of zebrafish,[60] we have removed it to perform the screening. Our results showed that 18 NP formulations had impact in the angiogenesis of the intersegmental vessels of zebrafish embryos. Most of the formulations (15 out 18) were confirmed by the *in vitro* tests.

The iPSC-derived vascular networks described here might be useful to screen other types of nano-biointeractions. For

example, recent studies have shown that some NPs can disrupt the VE-cadherin interactions between endothelial cells (called nanoEL effect), being negative charged NPs the ones with the highest impact.[9, 61] For this purpose, we have tested the effect of silica NPs (formulation NP13) in a monolayer of N-iPSC ECs for 1 h after which we have evaluated its paracellular permeability against FITC-dextran and VE-cadherin interaction between cells by confocal microscopy (Figure S10, Supporting Information). Our results clearly show the sensitiveness of our iPSC-derived vascular network to the nanoEL effect.

4. Conclusions

We have developed personalized human *in vitro* platforms with variable level of complexity (2D, 3D and blood vessel on a chip formats) and ageing phenotype to evaluate the interaction of nanomaterials with the vascular system. Taking in account the toxicity as the main readout, the NP toxicity profile was dependent on the age and vascular network format, being the NPs less cytotoxic in the blood vessel on a chip format due to the protective effect of glycocalyx. The platform present here is very promising for high-throughput screenings of nano-bio interactions in the context of regenerative and therapeutic medicine.

5. Experimental Section

Nanomaterials library: characterization. The diameter and morphology of some of the nanomaterials were characterized using a PHILIPS CM-12 transmission electron microscope at 100 kV. Few microliters of an aqueous suspension of nanomaterials was placed on a 200-mesh copper grid coated with a Formvar film and then wiped off by a filter paper. The dried grid was then examined under an electron microscope. Additionally, the nanomaterials were analysed by photon correlation spectroscopy (PCS) using quasi-elastic light scattering equipment (Zeta-Pals™ Zeta Potential Analyzer, Brookhaven Instruments Corp., Holtsville, NY) and ZetaPlus™ Particle Sizing Software (version 4.03). The nanomaterials suspension (2 mL, 50 µg/mL in PBS or EGM-2 media containing FBS) was added to a cuvette and allowed to stabilize for 10 min and then analysed (3 times) at room temperature. Nanomaterials suspended in EGM-2 media were then centrifuged (8,000 g, 8 min.) and resuspended in 1 mM KCl (2 mL, 50 µg/mL), at 25 °C. The nanomaterials suspension was finally characterized by zeta potential analyses. All data were recorded with at least 5 runs (in triplicate) with a relative residual value (measure of data fit quality) of 0.03.

***In vivo* studies**. Zebrafish (*Danio rerio*) were maintained in accordance with Institutional and National animal care protocols, in a re-circulating system at 28 °C on a 14 h-light, 10 h-dark cycle, fed twice daily. Transgenic adult zebrafish [Tg(fli1a:EGFP)[γ1]][26] expressing enhanced green fluorescent protein (EGFP) under control of the *fli1* promotor were used in this work. Genders were housed separately until the day before breeding, then placed in tanks at a 2:1 male:female ratio. Fish

were left undisturbed overnight and fertilized embryos were collected 4 hours after the light was turned on the next morning. For each condition, a minimum of 20 embryos within 4 hours-post-fertilization (hpf) were manually dechorionated and randomly placed in glass petri dishes containing 10 mL embryo medium. NPs at 1 µg/mL were added to the embryo medium and incubated for 24 hours, after which embryos were fixed with 4% PFA at 4ºC overnight. Embryos were then washed twice with PBS. As a control, the same amount of vehicle (water) was used. For each experimental group a minimum of eight embryos were analysed for the number of ISV's along the anterior-posterior axis, the average length of the first 10 ISV's and the total length of ISV's. Different batches of embryos and pools of embryos from different mating pairs were used among different experiments. Images of the embryos embedded in 3% carboxymethyl cellulose were obtained in a Zeiss/P.A.L.M. Laser Dissecting Microscope equipped with a Fluar 5x/0.25 M27 objective. The number and length of ISVs was directly measured in each image by the same user in Image J software.

iPSC culture. HGPS-iPS cells were generated from skin fibroblasts of a HGPS patient and were kindly donated by Xavier Nissan.[15] N-iPSCs were generated from cord blood (hiPSCs K2, passages 32-35)[62] and were kindly donated by Ulrich Martin. Cells at passage 35-45 have been used for the differentiation studies. Both iPSCs were cultured on inactivated mouse embryonic fibroblasts (MEFs), as previously described.[12, 13, 45]

iPSCs: differentiation into SMCs. The differentiation of iPSCs into SMCs was performed through an intermediary embryoid body (EB) stage. Undifferentiated iPSCs were treated with type IV collagenase (2 mg/mL, Invitrogen) for 2 h and then transferred (2:1) to low attachment plates (Corning) containing differentiation medium [10 mL, 80% KO-DMEM, 20% FBS, 0.5% L-glutamine, 0.2% β-mercaptoethanol, 1% nonessential amino acids and 50 U/mL:50 mg/mL penicillin-streptomycin solution] to form EBs. EBs were cultured for 10 days at 37ºC, 5% CO_2 in a humidified atmosphere, with media changes every 3–4 days. CD34^{+} cells were isolated from EBs at day 10 by magnetic-activated cell sorting (MACS). Isolated cells were grown on 24-well plates coated with 0.1% gelatin and containing endothelial growth medium-2 (EGM-2) supplemented with retinoic acid (1 mM, Sigma).

iPSCs: differentiation into ECs. Undifferentiated iPSCs were treated with type IV collagenase (2 mg/mL, Invitrogen) for 1 h and then transferred to petri dishes coated with fibronectin (1 µg/cm^{2}, Calbiochem) and containing differentiation medium [10 mL of 50% Iscove´s modified Dulbecco´s medium (IMDM, Gibco), 50% F12 (Gibco), 5 mg/mL BSA (Sigma), 0.2% β-mercaptoethanol, 15 mg/mL transferrin (Sigma), 7 mg/mL Insulin (Sigma) and 50 U/mL penicillin-streptomycin (Lonza)]. The differentiation medium was supplemented with BMP4 (10 ng/mL, Peprotech) and FGF-basic (20 ng/mL, Peprotech). After 1.5 days, the medium was replaced by fresh differentiation medium supplemented with BMP4 (50 ng/mL) and FGF-basic

(20 ng/mL). After 5 days, the medium was further replaced by fresh differentiation medium supplemented with $VEGF_{165}$ (50 ng/mL, Peprotech), Tβ4 (100 ng/mL, Caslo) and SB431542 (10 µM, Tocris). At the end of day 10, the $PECAM1^+$ cells were selected by magnetic labelling, plated in 0.1% gelatin-coated dishes and cultured with EGM-2 medium supplemented with $VEGF_{165}$ (50 ng/mL) and SB431542 (10 µM). Medium was changed every 2-3 days.

Primary vascular cell culture. Human vascular smooth muscle cells (Lonza, CC-2579) were cultured in MCDB 131 medium (Gibco) supplemented with FBS (20% v/v, Gibco), L-glutamine (Gibco, 1 mM) and penicillin-streptomycin (50 U/mL, Lonza). Human umbilical artery endothelial cells (HUAECs) and human umbilical vein endothelial cells (HUVECs) were cultured in EGM-2 (Lonza). Cell cultures were maintained at 37 ºC, 5% CO_2 in a humidified atmosphere, with media changed every 2 days.

Cell characterization: immunofluorescence analyses. Cells were washed with PBS, fixed with 4% paraformaldehyde (Electron Microscopy Sciences) for 15 min at room temperature and washed again with PBS. Cells were permeabilized (when necessary) with 0.1% Triton for 10 min, blocked with 1% (w/v) BSA for 30 min and incubated for 1 h with primary antibodies specific: mouse anti-human heparan sulfate (10E4 epitope, US Biological), rabbit anti-human smooth muscle α-actin (Abcam), mouse anti-human calponin (calponin1, Santa Cruz Biotechnology), mouse anti-human PECAM1 (clone JC70A, Dako), mouse anti-human VE-Cadherin (Santa Cruz Biotechnology) and rabbit anti-human ZO-1 (Life Technologies). The binding of primary antibodies was detected with: goat anti-rabbit IgG Alexa 488, goat anti-mouse IgG Alexa 488 or goat anti-mouse IgG Alexa 555 (Life Technologies). Cell nuclei were stained with 4', 6'-diamidino-2-phenylindole (DAPI, Sigma) and the slides were examined in a LSM 710 confocal microscope (Zeiss) or in a high-content fluorescence microscope IN Cell 2200 (GE Healthcare). In case of heparan sulfate immunostaining, imageJ software was used to quantify the overall intensity of heparan sulfate normalized by the area of the image in, at least, 8 images per condition.

Cell characterization: flow cytometry analyses. Cells were dissociated with non-enzymatic cell dissociation buffer (Gibco) for 10 min, followed by gentle pipetting and washes in PBS with 5% FBS. Single cells were aliquoted in PBS with 5% FBS (between 100,000 and 150,000 cells were used per condition) and stained with either isotype controls or antigen-specific fluorescent-conjugated antibodies for 30 min at 4ºC. The following antibodies have been used: PECAM1 (eBioscience, 5 µL per 100 µL of cell suspension), CD105 (Miltenyi Biotec, 10 µL per 100 µL of cell suspension) and VEGFR2 (R&D Systems, 10 µL per 100 µL of cell suspension). The flow cytometry analyses were performed in a BD Accuri C6 and data analysis was performed with FlowJo_V10. Ten thousand events were collected in each run. The percentages showed in dot plots were calculated based on the isotype controls represented by light blue. Isotype controls had 1% overlap with the protein of interest.

Cell characterization: ROS levels. N-iPSC ECs and HGPS-iPS ECs cells were plated in a 96-well plate at a density of $2×10^4$ cells per well and cultured for 24 h before incubation with 5 µM CellROX® Deep Red (Invitrogen) for 2 h. Cells were then washed, fixed with 3.7% formaldehyde for 15 min at room temperature and washed two times with PBS. Images were taken from each well (9 images per well) using the IN cell Analyzer 2200 (IN Cell 2200, GE Healthcare) and analysed using the Analyzer Workstation software. For oxidative stress measurements the mean intensity of CellROX® Deep Red was registered in both cell nucleus and cytoplasm. The total value of the measured intensity was used and normalized according to cell area. Assays were performed in triplicates.

Cell characterization: quantitative real-time polymerase chain reaction (qRT-PCR) analyses. Total RNA was extracted with RNeasy Micro Kit (Qiagen) and immediately stored at -80ºC. RNA was quantified in a NanoDrop ND-1000 spectrophotometer (NanoDrop Technologies, Inc., USA) at 260 nm. The cDNA was reverse transcribed from 1 µg of total RNA using TaqMan reverse transcription reagents kit (Invitrogen) according to the manufacturer instructions. The cDNA obtained was stored at -20ºC until further analysis by real-time PCR was performed. Real-time PCR analyses were performed by using the fluorescent dye SYBR green (Applied Biosystems) or Taqman technology (Life Technologies) and the 7500 Fast Real Time PCR System (Applied Biosystems). Specific sets of primers were designed by SIGMA.

Table 2 - Set of primers and probe for Progerin (Taqman technology) used in this work:

Probe	Sense	Antisense
CGGGAGCCCAGAGCTCCCAGAA	TGAGTACAACCTGCGCTCAC	TGGCAGGTCCCAGATTACAT

Taqman PCR conditions: initial step at 50 ºC for 2 min; after another step at 95 ºC for 10 min; 45 cycles at 95 °C for 15 sec and at 60 ºC for 1 min. After amplification, melting curves were acquired and used to determine the specificity of PCR products.

Table 3 - Sets of primers designed by Sigma used in this work:

	Sense	Antisense
PECAM1	AGATACTCTAGAACGGAAGG	CAGAGGTCTTGAAATACAGG
CDH5	ACGGGATGACCAAGTACAGC	ACACACTTTGGGCTGGTAGG
SELE	AGCTTCCCATGGAACACAAC	CTGGGCTCCCATTAGTTCAA
GAPDH	AGCCACATCGCTCAGACACC	GTACTCAGCGCCAGCATCG
ICAM1	CAAGGCCTCAGTCAGTGTGA	CCTCTGGCTTCGTCAGAATC
IL8	CCTTGGCAAAACTGCACCTT	CTGGCCGTGGCTCTCTTG
KDR	GTACATAGTTGTCGTTGTAGG	TCAATCCCCACATTTAGTTC
KLF2	CGTTTGTAGATGACAATGA	AGAAGTTTCAGGTGACTGA
NRF2	AAGGGCCTTAATTTGTACT	ATAAAAACGAACCAGGTAG
VCAM1	ACTTGATGTTCAAGGAAGAG	TCCAGTTGAACATATCAAGC
VEGF	AGAAGGAGGAGGGCAGAATC	ACACAGGATGGCTTGAAGATG
vWF	TGTATCTAGAAACTGAGGCTG	CCTTCTTGGGTCATAAAGTC

SYBR Green PCR conditions: initial denaturation step at 94 ºC for 5 min; 40 cycles of denaturation at 94 °C for 30 sec, annealing at 60ºC for 33 sec and extension at 72 ºC for 30 sec. At the end was performed a final 7 min extension at 72 ºC. After amplification, melting curves were acquired and used to determine the specificity of PCR products.

Cell characterization: monocyte-EC adhesion assay. THP1 (1×10^6 cells/ml) were incubated with CFSE (5 µM, Molecular Probes) for 15 min at 37ºC and washed three times in culture medium to remove the unbound dye at the ratio of 1:2 for 30 min. iPSCs derived-ECs were cultured in 24-well plates until confluence. The cells were then treated with 10 nM TNF-α (Peprotech) a pro-inflammatory cytokine, for 6 h. Next, cells were washed 3 times in culture medium and co-cultured with CSFE-labeled THP1 monocytes. Then, cells were washed 3 times with PBS to remove unbound THP1 cells, nuclei were stained with Hoechst (Molecular Probes), and the images were acquired in the InCell Analyser HCA System (GE Healthcare) and analyzed by the corresponding software. For non-treated and TNF-α-treated cells the percentage of THP1 cells was calculated relative to the total number of nuclei counted for each field. Each condition was performed in triplicate and a minimum of 9 fields were acquired per each well; on average 500 cells were counted per each field.

Culture of vascular cells in flow conditions. A suspension of SMCs (derived from N-iPSCs or somatic human SMCs, 30 µL in MCDB 131 medium, in order to have 4.1×10^4 cells/cm^2) was applied in each channel of an Ibidi plate (µ-Slide VI ^{0,4} Luer, Ibidi) and allowed to flow inside by capillary force. After 1 h each channel was filled with MCDB 131 medium. Cells were maintained in static conditions at 37ºC, 5% CO$_2$ in a humidified atmosphere for 12 h, after which a suspension of ECs (N-iPSC ECs or HUAECs, 30 µL of EGM-2 medium, in order to have of 12.5×10^4 ECs/cm^2) was applied on top of SMCs. After 1 h, each

channel was filled with EGM-2 medium, and cells were maintained at 37ºC, 5% CO$_2$ in a humidified atmosphere for 4 h in static conditions. After 4 h, cells were perfused with EGM-2 medium at physiological flow rate (20 dyn/cm^2) using an Ibidi pump system.

Cell characterization: heparan sulfate analyses. ECs co-cultured with SMCs in a microfluidic system for 5 days were characterized for the expression of heparan sulfate. Cells were stained with heparan sulfate (10E4 Epitope, USBiological) and the overall intensity of heparan sulfate of each image was quantified using ImageJ software. In a parallel experiment, cells were treated with heparinase III (flavobacterium heparinum 0.5U/mL, Sigma) for 30 min and washed with EGM-2 medium. Cells treated with heparinase were then exposed to low density lipoprotein from human plasma complexed with DiI (DiI LDL, Invitrogen) at 20 µg/mL at 37ºC for 4 h. Cells were then washed and maintained with medium. Images were acquired in a InCell Analyser HCA System and analysed using the corresponding software.

Nanomaterials library: preparation. The following nanomaterials have been used: zinc oxide (Product Number: 8410DL, SkySpring NanoMaterials), agion® silver antimicrobial type AJ (Product Number: AJ10D, Sciessent LLC), silicon oxide (Product Number: 6807NM, SkySpring Nanomaterials, Inc.), silicon dioxide (Product Number: PL-SiOF, Plasmachem), titanium oxide (Product Number: 7910DL, SkySpring Nanomaterials, Inc.), Molday ION MI-750 (Product Number:CL-50Q01-6A-53, BioPAL), micromer®-greenF 25 nm-NH$_2$ (Product Number: 29-01-251), micromer®-greenF 25 nm-COOH (Product Number: 29-02-251), micromer®-greenF, 100 nm-NH$_2$ (Product Number: 29-01-102) and micromer®-greenF 100 nm-COOH (Product Number: 29-02-102, Micromod Partikeltechnologie GmbH). The nanomaterials including 1.4MS-Au NPs, 1.5GSH-Au NPs, 12GSH-Au NPs, 13.9MS-Au NPs and 15MS-Au NPs were provided by Ulrich Simon group and the synthesis and characterization has been reported elsewhere.[25, 63, 64] PLGA,[20] PLGA-PS,[20] CM-AuNPs,[19] LL37-AuNPs,[18] PEI:DS,[21] PEI-DMNC,[24] A1,[22] A9,[22] C11,[22] E1,[22] E2,[22] P1C5,[23] P1C7[23] have been synthesized by us and the synthesis protocols previously published. 5HA-Au NPs were obtained by ligand exchange of 1.4MS-Au NPs with thiol end-modified HA. 20HA-Au NPs were obtained by ligand exchange of citrate-Au NPs (10 nm) with thiol end-modified HA. Thiol end-modified HA was obtained by reductive amination. Briefly, HA (MW 8-15 kDa, 100 mg) and cystamine dihydrochloride (60 mg) were dissolved in 0.1 M borate buffer (10 mL, pH 8.5) with 0.4 M NaCl and stirred for 2h. NaBH$_3$CN was added to the solution at a final concentration of 200 mM and reacted at 40 ºC for 5 days. The reaction mixture was incubated with 100 mM DTT for 12 h to introduce a free thiol group. The mixture was dialyzed (MWCO: 2 kDa) during 4 days (2 days against 100 mM of NaCl, 25% ethanol for 1 day and pure water for 1 day). The purified end-thiol modified HA was freeze-dried for 2 days and characterized by ^{1}H NMR and

Ellman's assay. The formation of HA-Au NPs was assessed by UV-Vis spectra, TEM, elemental analysis and DLS.

Toxicity of nanomaterials in iPSC-ECs cultured in 2D. N-iPSC ECs were seeded the day before the experiment at a density of 1×10^5 cells/cm^2 into 96 or 384 well plates. Nanomaterials suspended in water at 1mg/mL were added to cells at a concentration between 6 to 50 μg/mL for 24 h. In control the same amount of water without NPs was added to the cells. After 24 h incubation, cell viability was assessed by PrestoBlue® assay and apoptosis levels were monitored by propidium iodide (PI)/Hoechst 33342 staining. PrestoBlue assay is based on a resazurin-based solution that indicates the reducing power of living cells and therefore measures indirectly their number. Hoechst 33342, a blue-fluorescence dye (excitation/emission maxima at 350/461 nm, when bound to DNA), stains the condensed chromatin in apoptotic cells more brightly than the chromatin in normal cells and PI is a red-fluorescence dye (excitation/emission maxima ~535/617 nm when bound to DNA), is only permeant to dead cells. For each measurement, cell medium was removed, PI/Hoechst (10 μM) was added in EGM-2 medium and incubated for 10 min, after which the apoptosis levels were checked by microscopy by verifying the co-localization of the PI and Hoechst signals. Cells were then washed twice with PBS and a PrestoBlue solution (10% v/v, in EGM-2 medium) was added for 2 h at 37ºC, upon which the fluorescence was measured in a synergy H1 multi-mode reader (BioTek) at 590 nm with excitation at 560 nm.

ICP-MS analyses. NP internalization was monitored by ICP-MS. In this case, the intracellular levels of Zn (in ZnO, PEI-DS, PEI-DMNC, A1, C11 and P1C5 NPs), Ag (in Ag NPs) or Au (in LL37-Au, CM-Au and 1.4MS-Au NPs) were measured after N-iPSC ECs and HGPS-iPSC ECs exposure to NPs for 24 h (with the exception of 1.4MS-Au NPs which were only incubated for 4 h; longer incubation times would result in cell death) at a density of 1×10^5 cells/cm^2 in 96 or 384-well plates. After incubations, NPs that were not internalized by the cells were washed (three times with PBS) and the cells were then lysed, collected and lyophilized. The samples were analysed by ICP-MS for the concentration of intracellular levels of Zn, Ag or Au, depending on the NP composition. To convert the concentration of each element into a concentration of NP, a suspension of NPs (not exposed to cells) was also quantified by ICP-MS. Finally, the concentration of NP per cell was calculated.

Toxicity of nanomaterials in iPSC-ECs cultured in 3D. A 96 multiwell plate was coated with Matrigel (BD) (50 μL/well – Matrigel was thawed at 4ºC and both tips and plates were kept cold during the procedure) and placed at 37 ºC for 30 min. Cells were seeded on top of the polymerized Matrigel at a density of 2×10^3 cells/well together with nanoparticles (12.5 μg/mL) in EGM-2 medium (100 μL). After 24 h, bright field images were acquired in an InCell Analyser HCA System, and capillary-like networks analyzed using an Ibidi ACAS image software.

Toxicity of nanomaterials in a blood vessel on a chip. The effect of NPs was evaluated under flow conditions. N-iPSC ECs and N-iPSC SMCs cells were co-cultured as described in *Culture of vascular cells in flow conditions* section for 5 days in a microfluidic system. Cells were then washed and perfused with NPs at 50 μg/mL in EGM-2 medium at physiological flow rate (20 dyn/cm^2) for 24 h. Cell viability was assessed as described above for static conditions.

Statistical analyses. An unpaired t test or one-way ANOVA analysis of variance with Bonferroni post-test was performed for statistical tests. Results were considered statistically different when P<0.05. Data is shown as mean ± SEM.

Conflicts of interest

In accordance with our policy on Conflicts of interest please ensure that a conflicts of interest statement is included in your manuscript here. Please note that this statement is required for all submitted manuscripts. If no conflicts exist, please state that "There are no conflicts to declare".

Acknowledgements

References

1. D. M. Smith, J. K. Simon and J. R. Baker, Jr., *Nat Rev Immunol*, 2013, **13**, 592-605.
2. G. V. Lowry, A. Avellan and L. M. Gilbertson, *Nat Nanotechnol*, 2019, **14**, 517-522.
3. Z. Zhang, X. Li, J. Yin, Y. Xu, W. Fei, M. Xue, Q. Wang, J. Zhou and W. Guo, *Nat Nanotechnol*, 2018, **13**, 1109-1119.
4. S. J. Hawkins, L. A. Crompton, A. Sood, M. Saunders, N. T. Boyle, A. Buckley, A. M. Minogue, S. F. McComish, N. Jimenez-Moreno, O. Cordero-Llana, P. Stathakos, C. E. Gilmore, S. Kelly, J. D. Lane, C. P. Case and M. A. Caldwell, *Nat Nanotechnol*, 2018, **13**, 427-433.
5. L. Ye, K. T. Yong, L. Liu, I. Roy, R. Hu, J. Zhu, H. Cai, W. C. Law, J. Liu, K. Wang, J. Liu, Y. Liu, Y. Hu, X. Zhang, M. T. Swihart and P. N. Prasad, *Nat Nanotechnol*, 2012, **7**, 453-458.

6. K. Yamashita, Y. Yoshioka, K. Higashisaka, K. Mimura, Y. Morishita, M. Nozaki, T. Yoshida, T. Ogura, H. Nabeshi, K. Nagano, Y. Abe, H. Kamada, Y. Monobe, T. Imazawa, H. Aoshima, K. Shishido, Y. Kawai, T. Mayumi, S. Tsunoda, N. Itoh, T. Yoshikawa, I. Yanagihara, S. Saito and Y. Tsutsumi, *Nat Nanotechnol*, 2011, **6**, 321-328.

7. M. Faria, M. Bjornmalm, K. J. Thurecht, S. J. Kent, R. G. Parton, M. Kavallaris, A. P. R. Johnston, J. J. Gooding, S. R. Corrie, B. J. Boyd, P. Thordarson, A. K. Whittaker, M. M. Stevens, C. A. Prestidge, C. J. H. Porter, W. J. Parak, T. P. Davis, E. J. Crampin and F. Caruso, *Nat Nanotechnol*, 2018, **13**, 777-785.

8. B. Fadeel, L. Farcal, B. Hardy, S. Vazquez-Campos, D. Hristozov, A. Marcomini, I. Lynch, E. Valsami-Jones, H. Alenius and K. Savolainen, *Nat Nanotechnol*, 2018, **13**, 537-543.

9. M. I. Setyawati, C. Y. Tay, S. L. Chia, S. L. Goh, W. Fang, M. J. Neo, H. C. Chong, S. M. Tan, S. C. Loo, K. W. Ng, J. P. Xie, C. N. Ong, N. S. Tan and D. T. Leong, *Nat Commun*, 2013, **4**, 1673.

10. N. Bayat, V. R. Lopes, J. Scholermann, L. D. Jensen and S. Cristobal, *Biomaterials*, 2015, **63**, 1-13.

11. A. P. Sommer, *Circ Res*, 2010, **106**, e10.

12. H. Vazao, S. Rosa, T. Barata, R. Costa, P. R. Pitrez, I. Honorio, M. R. de Vries, D. Papatsenko, R. Benedito, D. Saris, A. Khademhosseini, P. H. Quax, C. F. Pereira, N. Mercader, H. Fernandes and L. Ferreira, *Proceedings of the National Academy of Sciences of the United States of America*, 2017, **114**, E3022-E3031.

13. S. Rosa, C. Praca, P. R. Pitrez, P. J. Gouveia, X. L. Aranguren, L. Ricotti and L. S. Ferreira, *Sci Rep*, 2019, **9**, 3826.

14. J. Ribas, Y. S. Zhang, P. R. Pitrez, J. Leijten, M. Miscuglio, J. Rouwkema, M. R. Dokmeci, X. Nissan, L. Ferreira and A. Khademhosseini, *Small*, 2017, **13**.

15. X. Nissan, S. Blondel, C. Navarro, Y. Maury, C. Denis, M. Girard, C. Martinat, A. De Sandre-Giovannoli, N. Levy and M. Peschanski, *Cell reports*, 2012, **2**, 1-9.

16. A. De Sandre-Giovannoli, R. Bernard, P. Cau, C. Navarro, J. Amiel, I. Boccaccio, S. Lyonnet, C. L. Stewart, A. Munnich, M. Le Merrer and N. Levy, *Science*, 2003, **300**, 2055.

17. K. Cao, C. D. Blair, D. A. Faddah, J. E. Kieckhaefer, M. Olive, M. R. Erdos, E. G. Nabel and F. S. Collins, *The Journal of clinical investigation*, 2011, **121**, 2833-2844.

18. M. Comune, A. Rai, K. K. Chereddy, S. Pinto, S. Aday, A. F. Ferreira, A. Zonari, J. Blersch, R. Cunha, R. Rodrigues, J. Lerma, P. N. Simoes, V. Preat and L. Ferreira, *Journal of controlled release : official journal of the Controlled Release Society*, 2017, **262**, 58-71.

19. A. Rai, S. Pinto, T. R. Velho, A. F. Ferreira, C. Moita, U. Trivedi, M. Evangelista, M. Comune, K. P. Rumbaugh, P. N. Simoes, L. Moita and L. Ferreira, *Biomaterials*, 2016, **85**, 99-110.

20. R. S. Gomes, R. P. das Neves, L. Cochlin, A. Lima, R. Carvalho, P. Korpisalo, G. Dragneva, M. Turunen, T. Liimatainen, K. Clarke, S. Yla-Herttuala, C. Carr and L. Ferreira, *ACS nano*, 2013, **7**, 3362-3372.

21. J. Maia, T. Santos, S. Aday, F. Agasse, L. Cortes, J. O. Malva, L. Bernardino and L. Ferreira, *ACS nano*, 2011, **5**, 97-106.

22. J. Blersch, V. Francisco, C. Rebelo, A. Jimenez-Balsa, H. Antunes, S. Pinto, S. Simoes, A. Rai and L. Ferreira, *Nanoscale*, 2020, **12**, 9935-9942.

23. J. Blersch, V. Francisco, C. Rebelo, A. Jimenez-Balsa, H. Antunes, C. Gonzato, S. Pinto, S. Simoes, K. Liedl, K. Haupt and L. Ferreira, *Angew Chem Int Ed Engl*, 2020, **59**, 1985-1991.

24. C. Boto, E. Quartin, Y. Cai, A. Martin-Lorenzo, M. B. G. Cenador, S. Pinto, R. Gupta, T. Enver, I. Sanchez-Garcia, D. Hong, R. Pires das Neves and L. Ferreira, *Nat Commun*, 2017, **8**, 15204.

25. Y. Pan, S. Neuss, A. Leifert, M. Fischler, F. Wen, U. Simon, G. Schmid, W. Brandau and W. Jahnen-Dechent, *Small*, 2007, **3**, 1941-1949.

26. N. D. Lawson and B. M. Weinstein, *Developmental biology*, 2002, **248**, 307-318.

27. S. Isogai, M. Horiguchi and B. M. Weinstein, *Developmental biology*, 2001, **230**, 278-301.

28. B. L. Roman, V. N. Pham, N. D. Lawson, M. Kulik, S. Childs, A. C. Lekven, D. M. Garrity, R. T. Moon, M. C. Fishman, R. J. Lechleider and B. M. Weinstein, *Development*, 2002, **129**, 3009-3019.

29. A. V. Gore, K. Monzo, Y. R. Cha, W. Pan and B. M. Weinstein, *Cold Spring Harbor perspectives in medicine*, 2012, **2**, a006684.

30. K. T. Kim and R. L. Tanguay, *Environmental health and toxicology*, 2014, **29**, e2014021.

31. K. J. Ong, T. J. MacCormack, R. J. Clark, J. D. Ede, V. A. Ortega, L. C. Felix, M. K. Dang, G. Ma, H. Fenniri, J. G. Veinot and G. G. Goss, *PloS one*, 2014, **9**, e90650.

32. Y. Pan, A. Leifert, D. Ruau, S. Neuss, J. Bornemann, G. Schmid, W. Brandau, U. Simon and W. Jahnen-Dechent, *Small*, 2009, **5**, 2067-2076.

33. A. Gojova, B. Guo, R. S. Kota, J. C. Rutledge, I. M. Kennedy and A. I. Barakat, *Environmental health perspectives*, 2007, **115**, 403-409.

34. S. Liang, K. Sun, Y. Wang, S. Dong, C. Wang, L. Liu and Y. Wu, *Chemico-biological interactions*, 2016, **258**, 40-51.

35. J. Sun, S. Wang, D. Zhao, F. H. Hun, L. Weng and H. Liu, *Cell biology and toxicology*, 2011, **27**, 333-342.

36. Y. Gong, Y. Ji, F. Liu, J. Li and Y. Cao, *Journal of applied toxicology : JAT*, 2017, **37**, 895-901.

37. Y. Gu, S. Cheng, G. Chen, Y. Shen, X. Li, Q. Jiang, J. Li and Y. Cao, *Toxicology mechanisms and methods*, 2017, **27**, 191-200.

38. M. Filipova, O. K. Elhelu, S. H. De Paoli, Z. Fremuntova, T. Mosko, D. Cmarko, J. Simak and K. Holada, *PloS one*, 2018, **13**, e0206557.

39. P. Nowak-Sliwinska, K. Alitalo, E. Allen, A. Anisimov, A. C. Aplin, R. Auerbach, H. G. Augustin, D. O. Bates, J. R. van Beijnum, R. H. F. Bender, G. Bergers, A. Bikfalvi, J. Bischoff, B. C. Bock, P. C. Brooks, F. Bussolino, B. Cakir, P. Carmeliet, D. Castranova, A. M. Cimpean, O. Cleaver, G. Coukos, G. E. Davis, M. De Palma, A. Dimberg, R. P. M. Dings, V. Djonov, A. C. Dudley, N. P. Dufton, S. M. Fendt, N. Ferrara, M. Fruttiger, D. Fukumura, B. Ghesquiere, Y. Gong, R. J. Griffin, A. L. Harris, C. C. W. Hughes, N. W. Hultgren, M. L. Iruela-Arispe, M. Irving, R. K. Jain, R. Kalluri, J. Kalucka, R. S. Kerbel, J. Kitajewski, I. Klaassen, H. K. Kleinmann, P. Koolwijk, E. Kuczynski, B. R. Kwak, K. Marien, J. M. Melero-Martin, L. L. Munn, R. F. Nicosia, A. Noel, J. Nurro, A. K. Olsson, T. V. Petrova, K. Pietras, R. Pili, J. W. Pollard, M. J. Post, P. H. A. Quax, G. A. Rabinovich, M. Raica, A. M. Randi, D. Ribatti, C. Ruegg, R. O. Schlingemann, S. Schulte-Merker, L. E. H. Smith, J. W. Song, S. A. Stacker, J. Stalin, A. N.

Stratman, M. Van de Velde, V. W. M. van Hinsbergh, P. B. Vermeulen, J. Waltenberger, B. M. Weinstein, H. Xin, B. Yetkin-Arik, S. Yla-Herttuala, M. C. Yoder and A. W. Griffioen, *Angiogenesis*, 2018, **21**, 425-532.

40. B. Yap, G. Garcia-Cardena and M. A. Gimbrone, *FASEB*, 2008, **22**, 471.411.

41. N. Kubben, W. Zhang, L. Wang, T. C. Voss, J. Yang, J. Qu, G. H. Liu and T. Misteli, *Cell*, 2016, **165**, 1361-1374.

42. J. M. Tarbell and L. M. Cancel, *J Intern Med*, 2016, **280**, 97-113.

43. J. Han, B. J. Zern, V. V. Shuvaev, P. F. Davies, S. Muro and V. Muzykantov, *ACS nano*, 2012, **6**, 8824-8836.

44. P. R. Pitrez, L. Estronca, L. M. Monteiro, G. Colell, H. Vazão, D. Santinha, K. Harhouri, D. Thornton, C. Navarro, A.-L. Egesipe, T. Carvalho, R. L. Dos Santos, N. Lévy, J. C. Smith, J. P. de Magalhães, A. Ori, A. Bernardo, A. De Sandre-Giovannoli, X. Nissan, A. Rosell and L. Ferreira, *Nature Communications*, 2020, **11**, 4110.

45. H. Vazao, R. P. das Neves, M. Graos and L. Ferreira, *PloS one*, 2011, **6**, e17771.

46. S. Y. Shaw, E. C. Westly, M. J. Pittet, A. Subramanian, S. L. Schreiber and R. Weissleder, *Proceedings of the National Academy of Sciences of the United States of America*, 2008, **105**, 7387-7392.

47. G. Lee, C. N. Ramirez, H. Kim, N. Zeltner, B. Liu, C. Radu, B. Bhinder, Y. J. Kim, I. Y. Choi, B. Mukherjee-Clavin, H. Djaballah and L. Studer, *Nature biotechnology*, 2012, **30**, 1244-1248.

48. S. Blondel, A. L. Egesipe, P. Picardi, A. L. Jaskowiak, M. Notarnicola, J. Ragot, J. Tournois, A. Le Corf, B. Brinon, P. Poydenot, P. Georges, C. Navarro, P. R. Pitrez, L. Ferreira, G. Bollot, C. Bauvais, D. Laustriat, A. Mejat, A. De Sandre-Giovannoli, N. Levy, M. Bifulco, M. Peschanski and X. Nissan, *Cell Death Dis*, 2016, **7**, e2105.

49. W. J. Trickler, S. M. Lantz, R. C. Murdock, A. M. Schrand, B. L. Robinson, G. D. Newport, J. J. Schlager, S. J. Oldenburg, M. G. Paule, W. Slikker, Jr., S. M. Hussain and S. F. Ali, *Toxicological sciences : an official journal of the Society of Toxicology*, 2010, **118**, 160-170.

50. S. Gurunathan, K. J. Lee, K. Kalishwaralal, S. Sheikpranbabu, R. Vaidyanathan and S. H. Eom, *Biomaterials*, 2009, **30**, 6341-6350.

51. C. Gonzalez, H. Rosas-Hernandez, M. A. Ramirez-Lee, S. Salazar-Garcia and S. F. Ali, *Arch Toxicol*, 2016, **90**, 493-511.

52. K. Okahara, B. Sun and J. Kambayashi, *Arterioscler Thromb Vasc Biol*, 1998, **18**, 1922-1926.

53. J. Han, V. V. Shuvaev, P. F. Davies, D. M. Eckmann, S. Muro and V. R. Muzykantov, *Journal of controlled release : official journal of the Controlled Release Society*, 2015, **210**, 39-47.

54. M. Balcells, J. Martorell, C. Olive, M. Santacana, V. Chitalia, A. A. Cardoso and E. R. Edelman, *Circulation*, 2010, **121**, 2192-2199.

55. T. Ziegler, R. W. Alexander and R. M. Nerem, *Ann Biomed Eng*, 1995, **23**, 216-225.

56. B. Uhl, S. Hirn, R. Immler, K. Mildner, L. Mockl, M. Sperandio, C. Brauchle, C. A. Reichel, D. Zeuschner and F. Krombach, *ACS nano*, 2017, **11**, 1498-1508.

57. M. J. Cheng, R. Kumar, S. Sridhar, T. J. Webster and E. E. Ebong, *Int J Nanomedicine*, 2016, **11**, 3305-3315.

58. J. Gao, C. T. Mahapatra, C. D. Mapes, M. Khlebnikova, A. Wei and M. S. Sepulveda, *Nanotoxicology*, 2016, **10**, 1363-1372.

59. C. Bai and M. Tang, *Journal of applied toxicology : JAT*, 2020, **40**, 37-63.

60. S. Vranic, Y. Shimada, S. Ichihara, M. Kimata, W. Wu, T. Tanaka, S. Boland, L. Tran and G. Ichihara, *Int J Mol Sci*, 2019, **20**.

61. J. Wang, L. Zhang, F. Peng, X. Shi and D. Tai Leong, *Chemistry of Materials*, 2018, **30**, 9.

62. A. Haase, R. Olmer, K. Schwanke, S. Wunderlich, S. Merkert, C. Hess, R. Zweigerdt, I. Gruh, J. Meyer, S. Wagner, L. S. Maier, D. W. Han, S. Glage, K. Miller, P. Fischer, H. R. Scholer and U. Martin, *Cell Stem Cell*, 2009, **5**, 434-441.

63. A. Leifert, Y. Pan, A. Kinkeldey, F. Schiefer, J. Setzler, O. Scheel, H. Lichtenbeld, G. Schmid, W. Wenzel, W. Jahnen-Dechent and U. Simon, *Proceedings of the National Academy of Sciences of the United States of America*, 2013, **110**, 8004-8009.

64. J. Broda, J. Setzler, A. Leifert, J. Steitz, R. Benz, U. Simon and W. Wenzel, *Nanomedicine : nanotechnology, biology, and medicine*, 2016, **12**, 1409-1419.